Journal of Energy Storage 179 (2026) 123884

Contents lists available at ScienceDirect

Journal of Energy Storage

journal homepage: www.elsevier.com/locate/est

Research Papers

Hybrid energy-based model for Li-ion battery degradation using real residential operating data in PV-battery systems

Filippo Onori, Mosè Rossi *, Gabriele Comodi

Department of Industrial Engineering and Mathematical Sciences (DIISM), Marche Polytechnic University (UNIVPM), Via Brecce Bianche 12, Ancona, 60131, Italy

ARTICLE INFO

Keywords:
Energy storage systems
State-of-Health calculation
Li-ion battery aging model
Operational battery degradation
Hybrid data-driven and empirical approaches

ABSTRACT

Battery Energy Storage Systems are playing a central role in the energy transition, thanks to their ability to integrate non-programmable renewable sources and ensure stability and flexibility in electricity grids. However, repeated charge and discharge cycles cause degradation processes that reduce the available capacity and useful life of the system. Understanding and predicting the evolution of the State-of-Health is therefore essential to optimising their use and planning their replacement. Several degradation models have been proposed in the scientific literature, generally based on controlled cyclic tests or electrochemical parameters that are not always accessible during normal operation. Conversely, this study presents an energy-based degradation model derived from experimental data collected from batteries operating under actual residential load conditions. The model uses charge and discharge power, cumulative energy, and State-of-Charge as input variables. This approach allows the evolution of State-of-Health to be accurately estimated, obtaining an R^2 value of 96.55% and a Root-Mean-Square-Error of 0.0015 from comparison with real residential data. The model is therefore an effective tool for predictive monitoring and intelligent management of Battery Energy Storage Systems, promoting greater reliability and sustainability in the context of the energy transition.

1. Introduction

The energy transition required to achieve climate neutrality by 2050 is driving a profound transformation in electricity production, distribution, and consumption [1]. The increasing penetration of non-dispatchable renewable energy sources, such as solar and wind, introduces challenges related to intermittency, grid stability, and energy balancing. In this context, Battery Energy Storage Systems (BESSs) are recognised as key enabling technologies for flexibility, reliability, and efficiency in modern power systems [2,3], enabling renewable integration, grid resilience, and ancillary services such as peak shaving and load leveling.

Despite their strategic role, batteries are inherently affected by degradation processes that progressively reduce usable capacity and performance [4,5]. Battery degradation impacts both technical reliability and economic viability, influencing investment decisions, maintenance planning, and overall profitability [6,7]. Consequently, accurate assessment of State-of-Health (SoH) evolution under real operating conditions is essential for optimal energy management, lifetime extension, and reliable replacement planning.

From a system-level perspective, inaccuracies in degradation modelling directly affect dispatch optimisation, lifetime cost evaluation, and replacement strategies of BESSs. Application-specific operating profiles can significantly alter battery utilisation and aging behaviour: indeed, aggressive strategies may accelerate degradation, whereas conservative assumptions can lead to underutilisation and increased system costs [8]. However, most degradation models are derived from laboratory tests under controlled conditions, which do not capture the variability and irregularity of real-world operating profiles of grid-connected BESSs. Therefore, the use of realistic operating profiles is necessary for reliable technical and economic assessments.

The scientific literature generally distinguishes between calendar aging, driven by temperature, State-of-Charge (SoC), storage duration [9], and cyclic aging associated with cycling intensity, Depth of Discharge (DoD), and charging and discharging regimes [10]. While this separation is appropriate under controlled conditions, it often breaks down under real operating profiles, where high average SoC, frequent micro-cycling, and daily energy throughput coexist.

Indeed, real operating conditions can lead to the failure of traditional degradation models, as stated by Vetter et al. [11]. In stationary applications, linear degradation assumptions are not valid, since dominant

* Corresponding author.
E-mail address: mose.rossi@staff.univpm.it (M. Rossi).

https://doi.org/10.1016/j.est.2026.123884
Received 22 January 2026; Received in revised form 13 June 2026; Accepted 24 July 2026
Available online 5 August 2026

Nomenclature

R^2	Goodness of fit σ_{SoC}
SoC	variability
ε	Total error
ARERA	Italian Regulatory Authority for Energy, Networks and Environment
BESS	Battery Energy Storage System
BMS	Battery Management System
DoD	Depth-of-Discharge
EIS	Electrochemical Impedance Spectroscopy
EVs	Electric Vehicles
GAM	generalised additive models
MAE	Mean Absolute Error
PV	PhotoVoltaic
RF	Random Forest
RMSD	Root-Mean-Square Deviation
RMSE	Root-Mean-Squared Error
SEI	Solid Electrolyte Interphase
SoC	State-of-Charge
SOH	State-of-Health
x	Normalised cumulative energy

mechanisms evolve and operating conditions are non-constant. Compared to automotive use, grid-connected BESSs are characterised by frequent micro-cycles, long residence times at high SoC driven by PhotoVoltaic (PV) self-consumption, and ambient temperatures that are not actively controlled [11,12]. As a result, degradation modelling in the BESS sector spans empirical, semi-empirical, and physicochemical approaches, with hybrid formulations increasingly adopted to handle complex and non-stationary operating profiles [13]. Experimental evidence confirms the relevance of these effects. Collath et al. [5] identified temperature, average SoC, and storage duration as dominant stress factors for calendar aging in stationary batteries. Sordi et al. [13] showed that capacity losses exceeding 10% can occur after approximately one year at high temperature and near-full SoC, while losses remain limited at moderate temperature and mid-range SoC. Keil et al. [14] demonstrated that Solid Electrolyte Interphase (SEI) growth follows a power-law dependence on time, with extended SoC plateaus exceeding 20–30% of the usable capacity. Temperature-dependent transitions in dominant degradation mechanisms were further identified by Waldmann et al. [15].

Under repeated cycling, cyclic degradation overlaps with calendar aging and modifies its evolution. Schuster et al. [16] reported a transition to non-linear capacity fade at residual capacities of approximately 80%. Barcellona and Piegari [17] showed that, when cell temperature is actively controlled, cycle aging is not directly dependent on current rate, highlighting the dominant role of thermal conditions. To address the interaction between calendar and cyclic mechanisms, combined and semi-empirical models have been proposed. De Hoog et al. [18] and Schimpe et al. [19] demonstrated that such models can accurately reproduce degradation under realistic operating profiles, achieving low prediction errors over extended validation periods. However, many datasets exhibit a degradation trajectory characterised by a knee point, after which capacity loss accelerates sharply [20], thus challenging the validity of linear or quasi-linear formulations commonly adopted in dispatch and optimisation models. Micea et al. [21] proposed a SoH estimation model based on a second-order polynomial regression, which enables simple and efficient prediction of the remaining capacity and the battery's useful life. The SoH estimation error approached zero starting from the 60th cycle, with a maximum Root-Mean-Square Deviation (RMSD) of 10.5 cycles. This empirical approach is particularly useful in contexts with limited computational resources, where simplicity and computational efficiency are essential. Intermediate modelling approaches aim to balance physical fidelity and operational usability. Energy-based models proposed by Liu et al. [22], Maheshwari et al. [23], and Seger et al. [24] incorporate non-linearity through simplified formulations derived from experimental data. While these models improve lifetime prediction and economic assessment compared to linear approaches, they typically rely on limited scalar indicators and do not fully capture the combined effects of energy throughput, C_{rate} intensity, and SoC distribution under uncontrolled operating profiles. In parallel, data-driven approaches based on machine learning techniques have been increasingly adopted for SoH estimation. These methods, such as the integrated multiphysics feature-based framework proposed by Son et al. [25], exploit operational or diagnostic variables to capture complex nonlinear degradation patterns and can achieve high predictive accuracy in Li-ion battery applications. For instance, the framework demonstrated an impressive Root-Mean-Squared Error (RMSE) of 0.494% for SOH estimation across various datasets, significantly outperforming traditional methods. By integrating mechanical and impedance features, this approach improves accuracy compared to mechanical-only features (RMSE = 3.38%) and impedance-only features (RMSE = 1.44%). Moreover, recent efforts have specifically aimed at improving the interpretability of data-driven SoH models by relying on physically meaningful features, feature-selection strategies, or explainable machine-learning tools. Bao et al. [26] proposed an interpretable machine-learning framework for Li-ion battery SoH prediction based on Electrochemical Impedance Spectroscopy (EIS) and temporal features, using explainability tools to analyse the influence of degradation-related features on model predictions. Using EIS features, the model achieves a Mean Absolute Error (MAE) of 0.17 and an RMSE of 0.40. When combining features, the XG-Boost model improves significantly, reaching a MAE of 0.05. In addition, Tang et al. [27] developed an innovative aging prediction method for Li-ion batteries using a model migration approach combined with Bayesian Monte Carlo algorithms. This data-driven method significantly reduces the need for experimental tests, providing accurate predictions of aging trajectories by adapting models derived from accelerated aging data to real-world operating conditions. The proposed method was validated on three types of commercial batteries, with the results demonstrating its effectiveness. Specifically, when using data from the first 30 cycles of normal-speed aging, the method achieved predictions of the entire aging trajectories (up to 500 cycles) with an RMSE of less than 2.5% for all tested batteries. Furthermore, even when only using the first five cycles of data for model training, the prediction error remained below 5% across all the battery types tested. These contributions represent a significant step towards reducing the gap between purely black-box predictors and physically interpretable degradation models. However, it is important to note that such methods may not always offer a closed-form, continuous, and monotonic degradation law that is directly compatible with optimization frameworks and long-term system-level analyses.

Table 1 summarises a selection of representative degradation models, including both energy-based formulations and data-driven approaches, with particular focus on methods that are relevant for comparison with the approach proposed in this work and for system-level applications under real operating conditions. Within each of these categories, a wide range of alternative formulations has been proposed in the scientific literature, often differing in terms of parameterisation, required inputs, and level of physical detail.

It should be noted that this table does not aim to provide an exhaustive overview of all modelling approaches available in the scientific literature, but rather to highlight representative methods relevant for comparison and system-level applications.

Despite the extensive scientific literature on battery degradation modelling, there remains a clear gap between the complexity of aging phenomena and the need for accurate, computationally efficient models that can be applied to real-world operating profiles of BESSs. To the best of the authors' knowledge, this gap has not yet been fully addressed in

Table 1
Representative lithium-ion battery degradation models for real-world applications.

Reference	Model type	Required data	Advantages	Notes
[21], [22]	Empirical energy-throughput	Real-world cycling data; energy throughput	Simple; suitable for operational datasets; captures global nonlinear ageing	No explicit SoC, C_{rate} or temperature dependence; simplified assumption
[23]	Nonlinear empirical, MILP-compatible	Lab tests at controlled SoC and C_{rate}	High accuracy; captures SoC and current effects; suitable for scheduling	Requires extensive experiments; complex degradation surface
[24]	Simplified empirical, energy-based	SoC series; Rainflow counting; energy exchange	Lightweight; suitable for long-term planning and sizing	Linear approximation; partial loss of cycle-depth information; SoC implicit
[20], [28]	Physics-based	Electrochemical and thermal characterisation	Highest physical fidelity; captures local degradation mechanisms	High computational cost; not suited to system-level optimisation
[25], [26]	Data-driven (ML-based)	Operational data: SoC, current, voltage, temperature	Captures complex nonlinear degradation behaviour	Limited interpretability; limited direct integration into optimisation frameworks
[27]	Data-driven (Bayesian Monte Carlo)	Accelerated aging data (over charging, over discharging, large current rates)	High prediction accuracy with minimal data requirements for training	Accelerated degradation tests; requires migration of models to match normal-speed aging data

the context of real-world BESSs operation. In particular, few models simultaneously satisfy the key requirements for system-level applications, namely continuity, monotonicity with respect to both utilisation intensity and cumulative stress, physical interpretability of parameters, and direct integrability into operational and optimisation frameworks.

Empirical models often exhibit limited generalisation beyond their calibration conditions, whilst semi-empirical approaches typically rely on variables that are not always accessible during operation. Physicochemical models, although highly accurate, are generally unsuitable for annual or multi-year simulations due to their computational cost. Formulations based on energy and SoC–current variables offer promising alternatives; however, their ability to jointly capture the effects of energy throughput, C_{rate}, and SoC variability under uncontrolled operating conditions remains largely unexplored. In addition, alternative techniques based on regression and machine learning have been proposed to enforce structural properties such as smoothness, monotonicity, and interpretability. These include multivariate fractional polynomial regression, Generalised Additive Models (GAMs) with shape constraints, and monotonic machine learning models. Such approaches can effectively represent nonlinear degradation trends while ensuring well-behaved functional forms. However, they typically rely on predefined basis functions or constrained fitting procedures, which may reduce their flexibility in capturing complex interactions among multiple stress factors under highly variable real-world operating conditions.

In this context, there is a clear and strong need for an energy-based degradation model, specifically designed for residential BESSs grounded in both real operational data and models investigated in the literature to date, that extends beyond cumulative energy alone and explicitly incorporates real operating conditions, including current intensity and SoC variability; indeed, such a model would offer a more comprehensive representation of aging mechanisms, making it suitable for system-level optimisation and long-term planning. The main contributions of this work can be summarised as follows:

- development of a purely energy-based degradation model that explicitly accounts for cumulative energy, dynamic current stress, and SoC variability under real operating conditions.
- introduction of a distillation-based calibration strategy to transfer knowledge from a data-driven model to a continuous and physically interpretable empirical formulation.
- validation of the proposed approach on independent real-world BESSs datasets, including a quantitative comparison with state-of-the-art energy-based degradation models.

Compared with recent energy-based and optimisation-oriented degradation models, the proposed method advances the state-of-the-art in three main aspects. First, it extends conventional energy-throughput or rainflow-based formulations by incorporating dynamic current stress and SoC variability through variables directly available from Battery Management System (BMS) data. Second, unlike purely data-driven SoH estimators, the final output is a closed-form degradation law that preserves continuity, monotonicity, and physical interpretability, making it suitable for optimisation and long-term techno-economic analyses. Third, validation on independent real-world BESSs datasets demonstrates improved accuracy with respect to representative scientific literature models. Building on these contributions, the proposed approach combines a non-parametric data-driven teacher with an empirical energy-based formulation through a distillation mechanism. This allows nonlinear degradation patterns to be extracted from operational data without imposing a priori assumptions on their structure, while retaining an analytical form suitable for system-level applications.

The remainder of this document is organised as follows. Section 2 presents the combined data-driven and empirical energy-based model, which accounts for the non-linear degradation behaviour of Lithium-ion batteries. This section also describes the methodology and the real dataset used for model validation. Section 3 presents the results and discusses the comparison with real data and with other models available in the scientific literature. Finally, Section 4 concludes the paper by summarising the main findings and outlining possible future developments.

2. Materials & methods

This section describes the development, calibration, and validation phases of the proposed degradation model specifically designed for residential BESSs, informed by real operational data and existing literature, and able to account for current intensity and SoC variability rather than relying solely on cumulative energy. Subsection 2.1 presents the hybrid architecture of the model. This architecture combines a data-driven approach with a non-linear empirical formulation based on physical variables. Subsection 2.2 describes the operational data used in this study. It also details the pre-processing and feature extraction procedures, as well as the methodology adopted to train the data-driven model and to identify the parameters of the empirical model through the distillation mechanism.

Fig. 1 illustrates the methodological workflow adopted in this study. Starting from real operational data, the procedure includes data pre-processing and feature extraction. It then involves the parallel development of a data-driven model and an empirical energy-based model, followed by an optimisation phase based on distillation. Finally, the resulting hybrid model is validated on independent datasets and compared with degradation models available in the scientific literature.

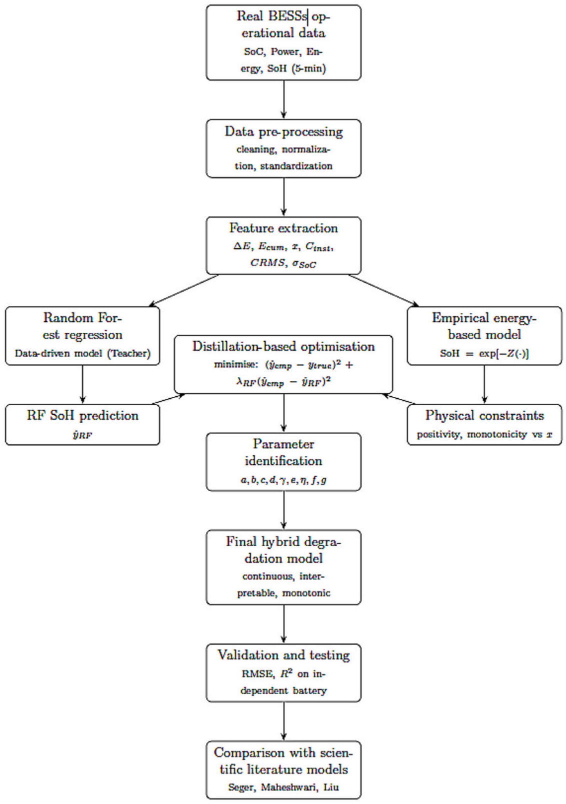

Fig. 1. Methodological workflow of the proposed hybrid energy-based battery degradation model.

2.1. Model development

This section describes the development of the proposed hybrid degradation model, detailing its mathematical formulation, the distillation-based calibration strategy, and the real-world dataset used for validation. The methodology is designed to ensure physical consistency, computational efficiency, and direct applicability to residential-scale system-level studies.

This work proposes a hybrid model of Lithium-ion battery degradation, which synergistically combines a data-driven approach, based on Random Forest (RF), and a non-linear empirical model constructed from physical variables observed during actual storage operation. This hybrid structure enables the capture of complex non-linearities emerging from the experimental data through RF, while providing a continuous and interpretable representation of the degradation mechanisms through empirical formulation. Unlike constrained regression approaches (e.g., GAMs or monotonic regression), the proposed framework does not require explicit specification of the functional structure of interactions among variables, as these are implicitly learned from data through the distillation process. The model allows for estimating the SoH of batteries during their operation.

The empirical contribution of the model has been formulated (see Eq. 1) to describe the SoH as an exponential decay:

$$\mathrm{SoH}_{\mathrm{DEL}} = \exp[-Z(x, C_{\mathrm{RMS}}, \sigma_{\mathrm{SoC}})] \tag{1}$$

The empirical degradation model uses only physical terms, which are defined as follows:

- x represents the cumulative energy normalised with respect to the nominal capacity of the battery. This variable is a direct measure of the energy use of the system and can be interpreted as a continuous equivalent of charge/discharge cycles. As x increases, the battery accumulates electric work performed, which correlates with cyclic aging and progressive loss of capacity. Eq. 2 shows how the value of x is calculated:

$$\sum \frac{|P(t)|\Delta t}{E_{\mathrm{nom}}} \tag{2}$$

where $P(t)$ is the instantaneous power at time t, Δt is the time interval, and E_{nom} is the nominal energy capacity of the battery.

- C_{RMS} is the root mean square value of C_{rate}, calculated over a time window of sufficient amplitude to describe dynamic stresses. The C_{rate} is defined as the ratio between the instantaneous power and the nominal energy capacity of the battery:

$$C_{rate} = \frac{P(t)}{E_{\mathrm{nom}}} \tag{3}$$

  The use of a root mean square measurement, rather than an average C_{rate} value, allows the actual electrical stress experienced by the cell to be captured, making it more sensitive to power peaks and impulsive fluctuations that have a significant impact on aging mechanisms. This indicator summarises the average intensity of short-term electrical stresses, reflecting the effects of rapid electrical stress, power transients, and impulsive load variations, which are known to accelerate degradation.
- σ_{SoC} represents the standard deviation of the SoC in the same moving window. It acts as a mixed proxy that incorporates both the effect of microcycles induced by rapid power variations and the influence of remaining at certain SoC levels. A high value of σ_{SoC} indicates an operating profile with repeated and aggressive variations, typical of applications with high power variability, e.g., PV coupled with battery, which contribute significantly to cell aging.
- a, b, c, d, γ, e, η, f, g are the empirical parameters to be identified through optimisation. They determine the relative weight of the various physical contributions to degradation:
  - a, b, c regulate the part of degradation associated with cumulative energy, linear and non-linear components.
  - d, γ model the sensitivity to dynamic power stress via C_{RMS}.
  - e, η describe the contribution due to SoC variability.
  - f, g are coupling terms that do not represent independent direct physical mechanisms, but model non-linear interactions observed in experimental data between cumulative energy and dynamic stresses, allowing for improved descriptive capacity of the model in the presence of combined aging phenomena.

The choice of an exponential formulation for the description of SoH is based on the interpretation of degradation as a process of irreversible cumulative damage. In this context, the exponential term allows for a compact representation of the progressive accumulation of aging effects, while ensuring a monotonic decrease in SoH and asymptotic behaviour consistent with the experimental evidence reported by Hennessy et al. [29] for Lithium-ion cells. The total degradation function was defined by Eq. 4:

$$Z = ax^b + cx + dC_{\mathrm{RMS}}^{\gamma} + e\sigma_{\mathrm{SoC}}^{\eta} + f(xC_{\mathrm{RMS}}) + g(x\sigma_{\mathrm{SoC}}) \tag{4}$$

To improve the robustness of the model and constrain empirical learning to physically plausible regions, a distillation mechanism based on the predictions of the data-driven RF model was adopted. Distillation is a technique widely used in machine learning to transfer knowledge from a complex and non-interpretable model, referred to as the teacher (in this case, the RF), to a simpler, continuous, and physically interpretable model, referred to as the student (in this case, the empirical model).

In this work, the RF model is trained independently using key operating variables as inputs, namely SoC, normalised power, and cumulative energy. Owing to its non-parametric nature, the RF can capture highly non-linear relationships present in real operating data. As a result, it provides a particularly accurate estimate of SoH on the training dataset. However, despite their statistical robustness, these predictions do not guarantee continuity, monotonicity, or behaviour consistent with the physical mechanisms of degradation. For this reason, the RF model cannot be used directly as the final degradation model. It is important to stress that the RF model is not used as the final degradation model in operational dispatch or optimisation studies. Its role is strictly limited to the identification of parameters based on distillation, guiding the calibration of the empirical formulation while ensuring that the final model remains continuous, monotonic, and physically interpretable. The adopted solution consists of using the RF model as a guiding signal during the identification of the empirical model parameters. In practice, the RF outputs inform the empirical model about which regions of the solution space are plausible based on the available data, without enforcing strict adherence. It is worth noting that the RF model does not introduce any physical causality into the process. Instead, it acts solely as a data-driven regulariser, providing a statistical constraint derived from observed data. This is achieved by introducing an additional term proportional to the distance between the empirical model prediction and the RF prediction. The total error minimised during optimisation therefore takes the following form:

$$\varepsilon = \left(y_{\text{emp}} - y_{\text{true}}\right) + \lambda_{\text{RF}} \left(y_{\text{emp}} - y_{\text{RF}}\right) \tag{5}$$

where:

- y_{true} is the actual measured SoH.
- y_{RF} is the RF model prediction.
- y_{emp} is the empirical model prediction.
- λ_{RF} is a weighting coefficient that balances the contribution of distillation; it does not bias the empirical model towards the RF estimations but penalises unstable regions of the solution space where data-driven estimates are inconsistent.

The first term of Eq. 5 enforces that the empirical model accurately approximates the experimental data. The second term introduces a regularisation constraint based on the RF predictions. In practice, the empirical model is guided towards regions of the prediction space where the RF model exhibits consistency and stability. At the same time, it retains sufficient freedom to preserve a physically meaningful structure and a causal interpretation.

The optimisation of the empirical parameters is performed by minimising a quadratic error function. This optimisation is subject to physical constraints on the parameters, including positivity of the coefficients and monotonicity with respect to cumulative energy. The iterative procedure is terminated when the objective function converges or when no significant improvement is observed after a predefined number of iterations. This strategy leads to a hybrid solution. On the one hand, the data-driven component captures complex patterns that cannot be directly represented by a simple analytical formulation. On the other hand, the empirical model ensures continuity, monotonicity, and physical interpretability. These properties are essential for a degradation model intended for use in real engineering and operational applications.

2.2. Methodology and real data

The degradation model was calibrated with real operating data from three Lithium Iron Phosphate ($LiFePO_4$) batteries under actual residential load conditions. The main characteristics of these batteries are as follows: nominal power of 2.56 kVA, energy capacity of 5.0 kWh, and a round-trip efficiency of 90%. Each battery has dimensions of 188 × 550 × 980 mm and a weight of 78.9 kg. Operating data from battery 1 were used for the training phase, data from battery 2 for validation, and data from battery 3 for testing.

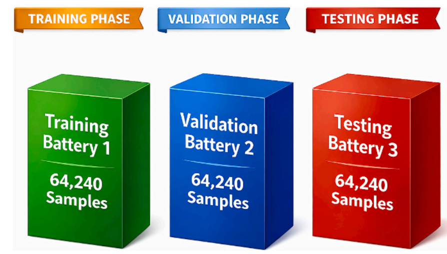

Fig. 2. Dataset partitioning across batteries.

Specifically, each battery was part of an independent residential PV-BESS, as shown in Figs. 3, 4, 5, and they were not connected to form a single unified system. However, although the batteries were physically distinct and used for training, validation, and testing, their operating conditions were representative of the same application class. In particular, all systems experienced daily charge/discharge patterns driven by PV production and household demand, with comparable consumption peaks and frequent power fluctuations typical of residential PV-coupled storage operation. During the monitored operation, the batteries never discharged below 20% of their total capacity. Additionally, it is important to note that the proposed model is specifically designed for residential PV-BESS systems and does not consider Electric Vehicles (EVs), as their charge and discharge cycles are highly variable and largely determined by user behaviour. EV charging often occurs within a few hours via fast charging, and discharging occurs during vehicle use, resulting in operational profiles that are very different from those of residential BESS-PV systems. Therefore, the analysis focuses solely on integrated PV-BESS systems, and the findings should be interpreted within this scope.

Figs. 3, 4, and 5 show representative operating profiles of the integrated PV-BESS systems for a significant day in each season, illustrating the relationship between PV production, consumption, and battery operation. These profiles are broadly similar across different batteries and days, with only minor variations, reflecting the standardized patterns of residential consumption reported by the Italian Regulatory Authority for Energy, Networks and Environment (ARERA) [30]. The charge and discharge cycles are almost always consistent: charging occurs mainly during daytime hours, when PV production generates an energy surplus and consumption is moderate, while discharging is concentrated in the evening, in the absence of PV generation, to meet residual demand. As shown in the figures, consumption peaks mostly occur in the evening, while battery charging follows the typical PV generation profile. Apart from some variations between users, these profiles are therefore highly repeatable and representative of residential PV-BESS systems.

Additionally, Fig. 6 displays the individual power profiles of the three batteries, highlighting their operating ranges and the recurring charge/discharge cycles, which are consistent across all three batteries. The values presented in these profiles are aggregated with an hourly resolution.

Together, these figures confirm that the datasets used in this analysis align with a typical, similar residential PV-BESS usage profile, while still capturing the inherent variability specific to each battery.

The datasets were used for parameter identification, selection of optimal configurations, and independent verification of model performance, respectively. Each dataset consists of a time series with a sampling interval of 5 min. For each time step, the dataset includes the following main variables: SoC, electrical power exchanged with the battery expressed in kW, exchanged energy expressed in kWh, and SoH.

The variables such as SoC, electrical power, and exchanged energy are directly provided by the BMS of the BESSs under investigation; therefore, these quantities represent real-time measurements, which are typically available in real-world operating systems.

In contrast, the SoH is not directly measured by the BMS but is

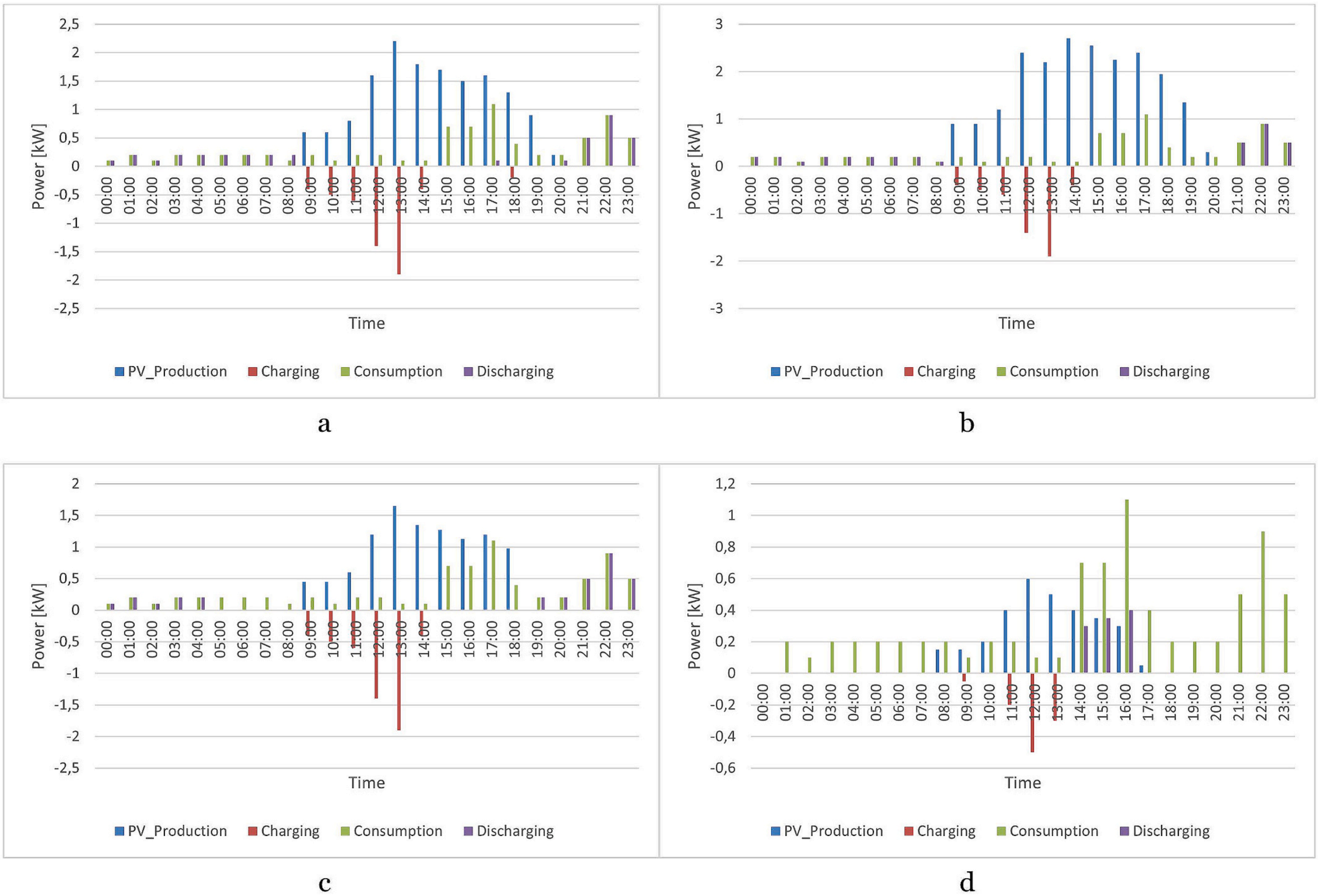

Fig. 3. Representative operating profiles of the integrated PV-BESSs for Battery 1: (a) Spring, (b) Summer, (c) Autumn, (d) Winter.

periodically assessed through a full charge-discharge test conducted monthly. This procedure enables the accurate measurement of the battery's actual available energy capacity, providing a reliable reference value for the SoH. While these tests are not continuously available during operation, they offer a high-precision benchmark for model calibration and validation. The full charge-discharge operations are represented in Fig. 6; however, since the time is shown along the X-axis, the exact timing of these operations is not explicitly indicated.

During the pre-processing phase, the datasets are standardised and cleaned. The columns are mapped to a set of standard names, and non-numeric or missing values are removed. The SoC and SoH variables are scaled to the range [0,1]. Electrical power is also converted to its absolute value. This operation is required to estimate the total energy exchanged, regardless of the charge or discharge direction. For each dataset, the quantities required by the empirical model are then derived:

- the elementary energy exchanged in the sampling step:

$$\Delta E(t) = |P(t)|\,\Delta t \tag{6}$$

- the cumulative energy as a sum over time:

$$E_{cum}(t) = \sum_{\tau=0}^{t} \Delta E(\tau) \tag{7}$$

- the dimensionless variable x, defined as cumulative energy normalised with respect to the nominal capacity of the battery, assumed to be 5 kWh, in accordance with Eq. 4;
- the instantaneous C_{rate}:

$$C_{\text{inst}}(t) = \frac{|P(t)|}{E_{\text{nom}}} \tag{8}$$

- the root mean square value of C_{rate}, calculated on a moving window of 288 samples, corresponding to 24 h, which summarises the average intensity of dynamic power stresses. It is worth noting that sensitivity analyses on shorter and longer windows showed no significant improvement in predictive accuracy, while increasing computational burden or reducing physical interpretability:

$$C_{\text{RMS}}(t) = \sqrt{\frac{1}{N}\sum_{k=t-N+1}^{t} C_{\text{inst}}^{2}(k)} \tag{9}$$

where $N = 288$, the choice of a 24-h rolling window is consistent with the typical daily cycle of PV-BESS. Specifically, several window sizes have been tested, namely 72, 144, 228, 576, and 864 samples, to assess the stability and performance of the model. The results indicate that the model remains robust across these different window lengths, with slight improvements in performance metrics as the window size increases. However, the 288-sample window provided the best performance improvement when compared to other window sizes. Fig. 7 shows how the performance metrics evolve with different rolling window sizes. The percentage improvement in performance metrics was evaluated using

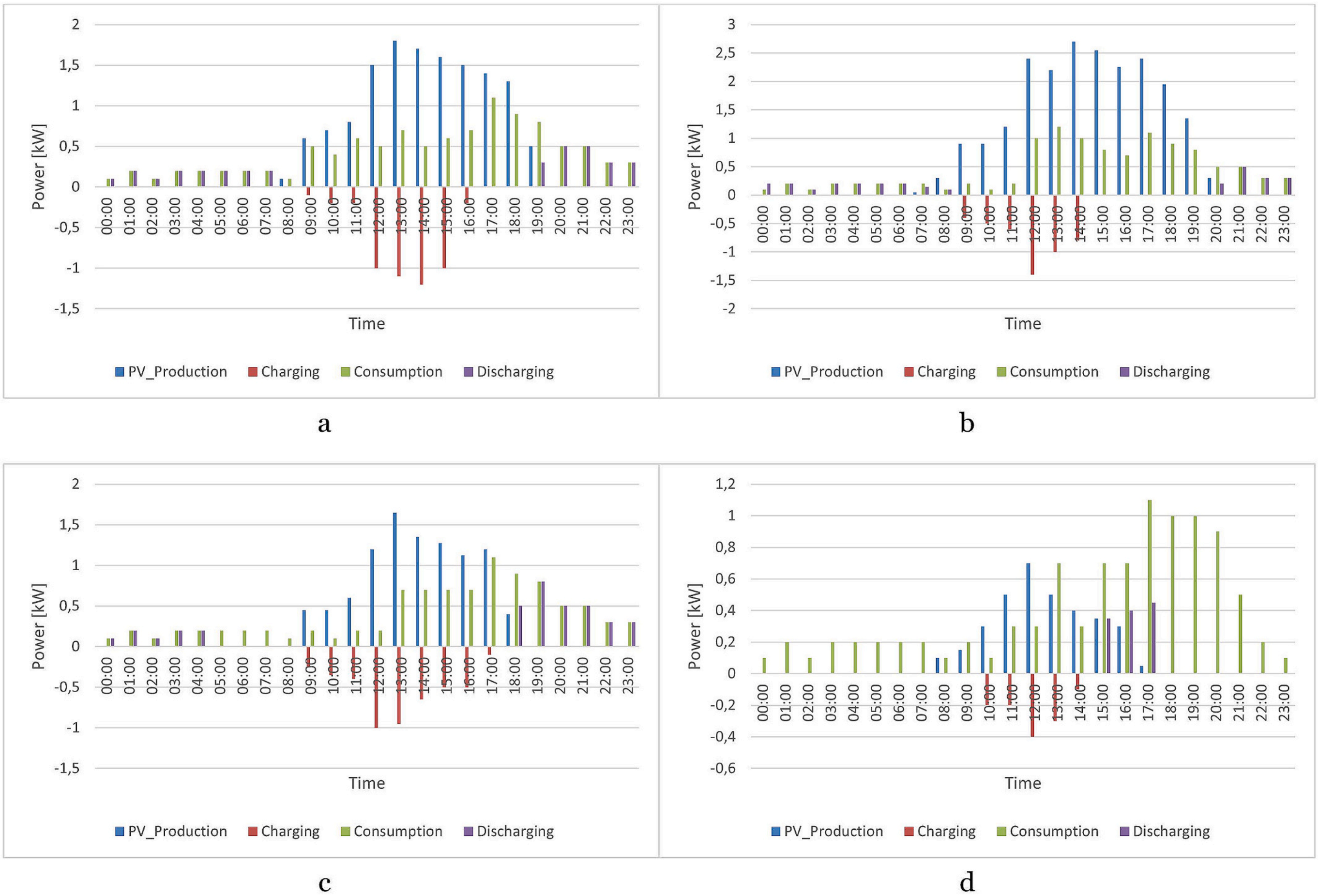

Fig. 4. Representative operating profiles of the integrated PV-BESSs for Battery 2: (a) Spring, (b) Summer, (c) Autumn, (d) Winter.

the following formula, according to the equation:

$$\text{Percentage} = \frac{X_{n+1} - X_n}{X_n} \times 100 \tag{10}$$

where X_n represents the value of a sample, and X_{n+1} represents the value of the next sample. This graph shows that the 288-sample window maximises performance improvements, demonstrating its suitability for capturing the day-night cycle, solar generation profiles, and energy management strategies typical of PV-BESSs.

- the standard deviation of SoC, calculated on the same moving window, which measures the amplitude of charge state oscillations and therefore the presence of internal micro–cycles:

$$\sigma_{\text{SoC}}(t) = \sqrt{\frac{1}{N-1} \sum_{k=t-N+1}^{t} \left(\text{SoC}(k) - \overline{\text{SoC}}\right)^2} \tag{11}$$

Unlike traditional cycle-counting approaches, these indicators capture degradation-relevant information directly from continuous power and SoC trajectories, without requiring offline rainflow analysis. These features constitute the inputs of the empirical formulation in Eq. 2, from which the exponential degradation term in Eq. 1 is derived. To improve numerical stability during the optimisation process, the variables C_{RMS} are further normalised with respect to their 95*th* percentile in the training dataset. This scaling reduces differences in magnitude among the individual contributions. Temperature is not explicitly included among the model input variables.

This choice is deliberate and motivated by the objective of maintaining applicability in real-world scenarios with limited sensor availability. The batteries used in this study were operated under passive thermal control, where natural convection was employed to dissipate heat, with the ambient temperature maintained within a range of 15–45 °C. No significant thermal stress was observed, contributing to the temperature secondary to the electrical effects analysed.

In parallel, an RF regression model is trained on the same operational dataset and used as the teacher in the distillation process. The RF model takes as input key quantities that are readily available during operation, namely, instantaneous SoC, normalised power with respect to a reference value, the 95*th* percentile of power in the training set, and cumulative electrical energy. It returns a point estimate of SoH. The RF is trained independently to maximise statistical accuracy on real data, without imposing constraints related to monotonicity or the physical structure of degradation. The empirical parameters $a, b, c, d, \gamma, e, \eta, f, g$ are identified using the training dataset for the primary fit, while the validation dataset is used to mitigate overfitting. The objective function minimised during calibration is the total error defined in Eq. 5. This error combines the distance between the empirical prediction and the measured SoH with a regularisation term that penalises deviations from the RF prediction. The regularisation term is weighted by the coefficient λ_{RF}.

In this study, λ_{RF} is set equal to 0.85. This value assigns a predominant weight to the ground truth data, while still exploiting the structural information provided by the data-driven model in regions where its predictions are most stable. The value of λ_{RF} was selected based on a sensitivity analysis. In this analysis, the weight of the distillation term was varied, and the model performance was evaluated in terms of R^2 on

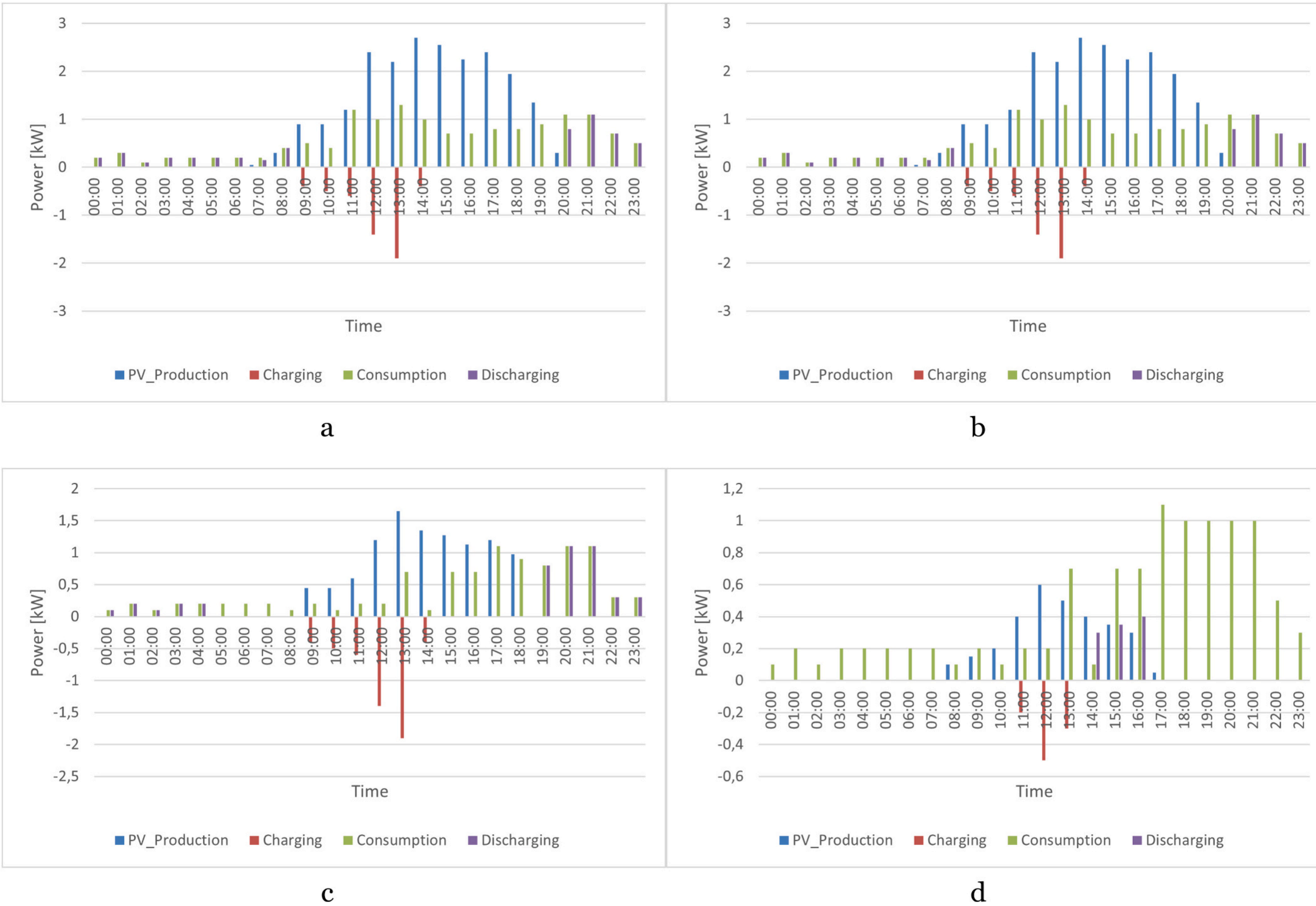

Fig. 5. Representative operating profiles of the integrated PV-BESSs for Battery 3: (a) Spring, (b) Summer, (c) Autumn, (d) Winter.

the validation dataset. Fig. 8 shows the trend of R^2 as the distillation weight varies. It is worth noting that the ground-truth data remains dominant in the hybrid model, thereby preserving physical interpretability and preventing an overemphasis on the data-driven predictions. This choice aligns with the model's goal of maintaining a balance between empirical knowledge and data-driven insights, ensuring that the underlying physical principles are not overshadowed by the predictions of the RF model.

Optimisation is performed in two stages. First, an initial global search is conducted in the parameter space, subject to physically plausible bounding constraints. This step is followed by a local refinement phase based on robust non-linear least-squares minimisation. The test dataset, corresponding to battery 3, is used exclusively for the final model validation. Performance indicators, including RMSE and R^2, are computed on the training, validation, and test datasets. In all cases, the measured SoH is compared with the estimates provided by both the distilled empirical model and the RF model. The joint analysis of error metrics and the temporal evolution of the SoH curves allows verification that the hybrid model achieves high predictive accuracy. At the same time, it preserves physically consistent and monotonic behaviour, which is essential for real engineering applications.

Finally, the effectiveness of the proposed model is assessed through a comparison with degradation models available in the scientific literature. These models are tested using the operational data from all three batteries. The models presented in [22], [23], and [24] are selected because they are energy-based formulations calibrated on real operational data. This choice ensures consistency with the datasets and conditions considered in the present study.

3. Results & comments

This section presents the key results obtained with the proposed model, including the identified parameters of the empirical formulation, its validation against real residential operating data, and a comparison with existing models reported in the scientific literature. These results demonstrate the effectiveness of the proposed hybrid approach.

3.1. Identification and interpretation of parameters

The parameter identification problem was formulated as a constrained non-linear optimisation task. The objective was to minimise the discrepancy between the measured SoH and the value predicted by the empirical degradation model on both the training and validation datasets. Due to the highly non-linear and non-convex nature of the exponential degradation formulation, a two-stage optimisation strategy was adopted.

In the first stage, a global optimisation algorithm based on differential evolution was used to explore the parameter space and identify a physically plausible initial solution. This approach is effective in avoiding convergence to local minima and ensures robustness with respect to the initial parameter estimates. In the second stage, the solution obtained from the global search was refined using a local non-linear least-squares optimisation. During this phase, a robust loss function was adopted to limit the influence of outliers and measurement noise, which are commonly present in real battery datasets. This refinement step improves the accuracy of the parameter estimates while preserving numerical stability. During optimisation, each parameter was constrained within predefined bounds. These bounds were introduced to

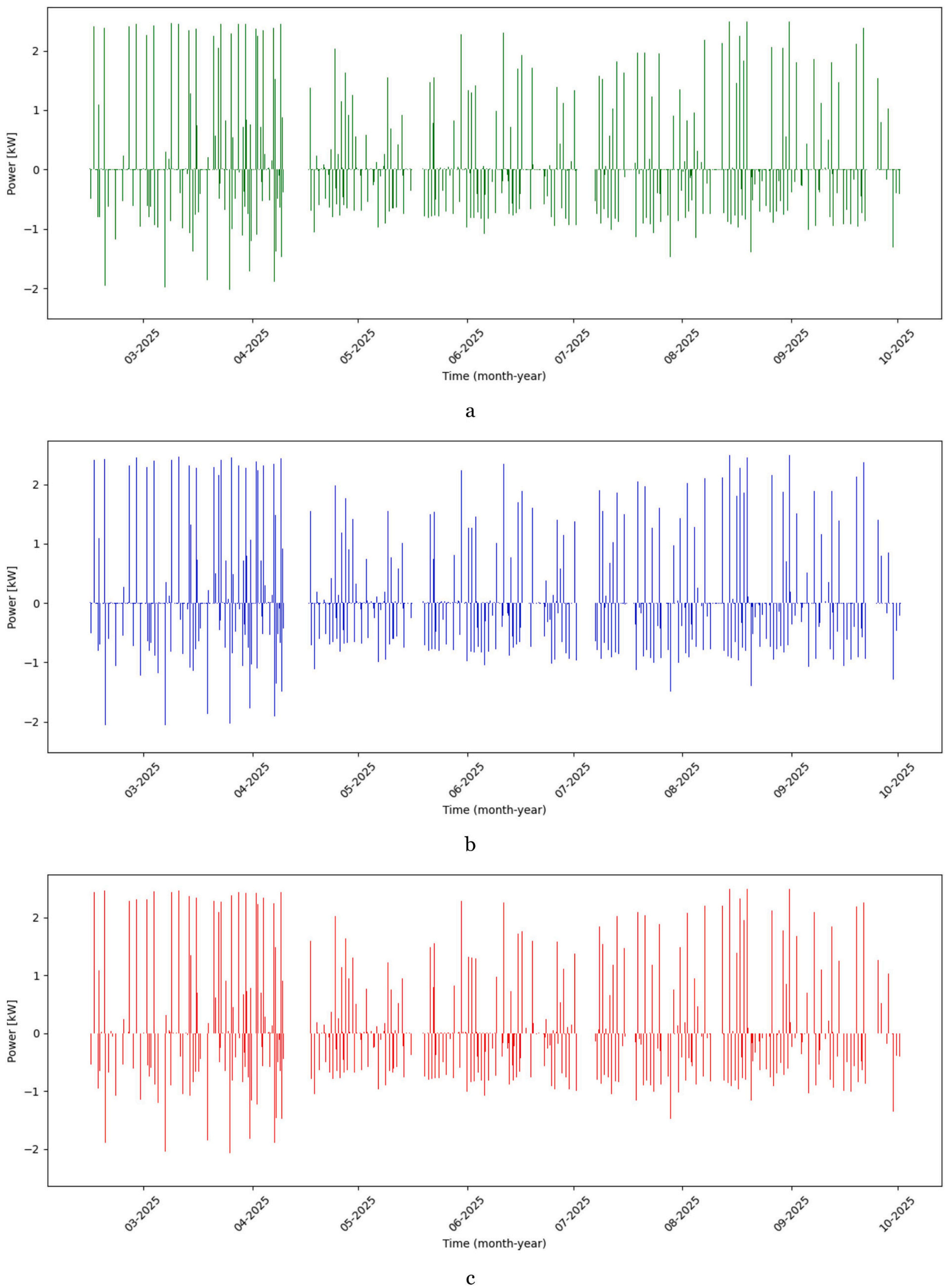

Fig. 6. Power profiles of the three independent batteries: (a) Battery 1, (b) Battery 2, (c) Battery 3.

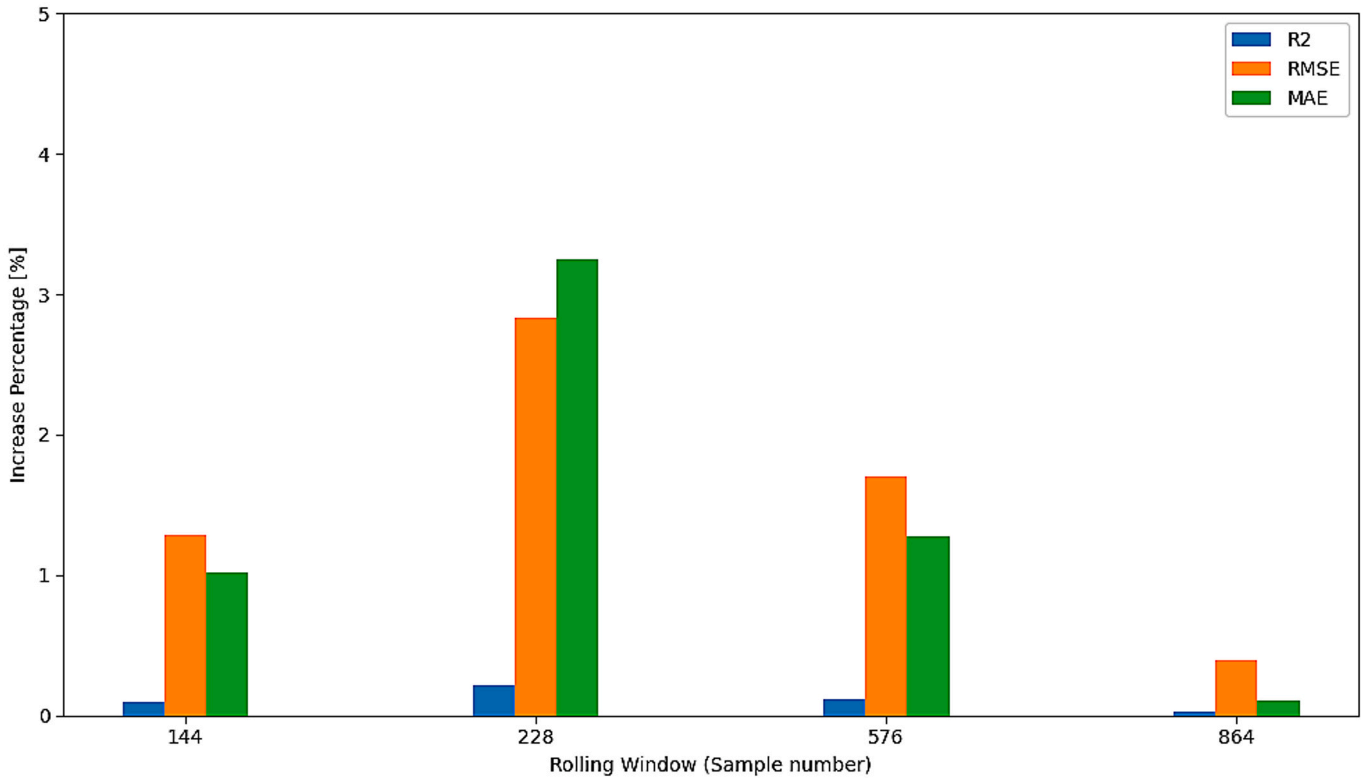

Fig. 7. Sensitivity analysis of rolling window.

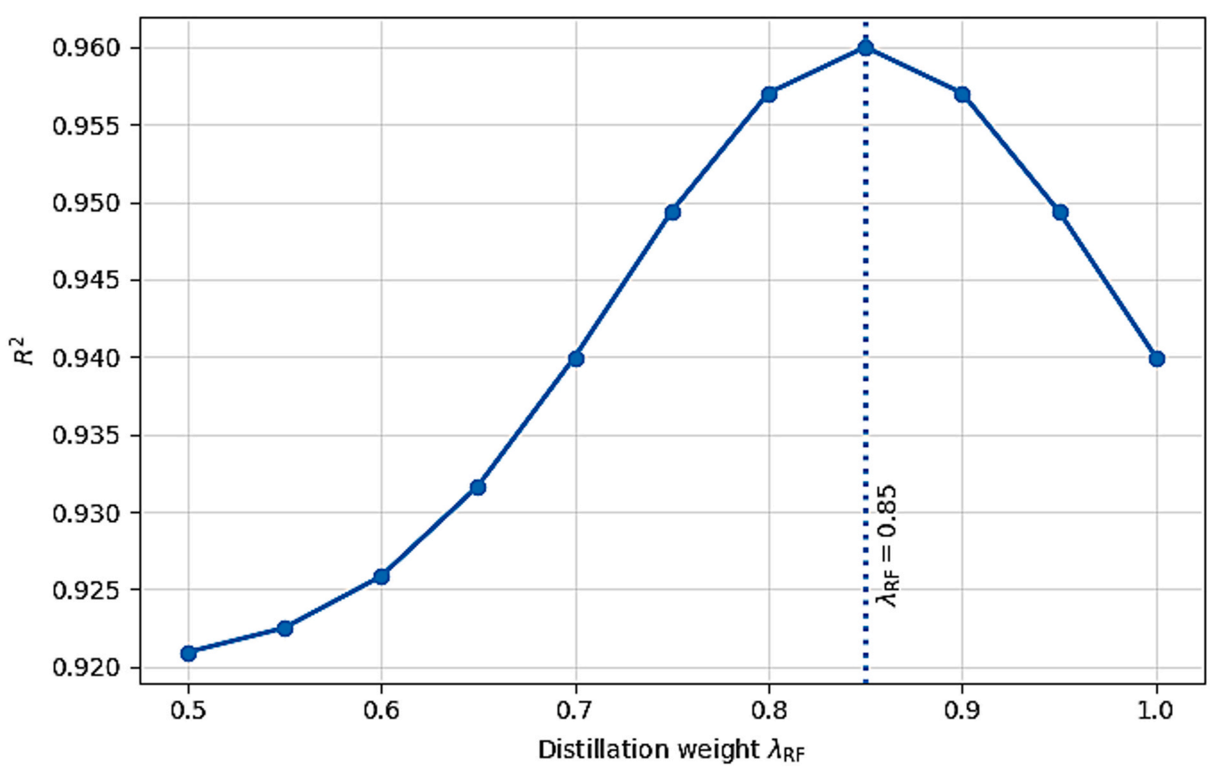

Fig. 8. Sensitivity analysis of R^2 to the distillation weight λ_{RF}.

ensure the physical consistency of the degradation mechanisms, the numerical stability of the exponential formulation, and robustness against overfitting. The selected limits reflect plausible ranges commonly adopted in empirical battery aging models and are reported in Table 2. In particular, positive lower bounds on the exponents b, γ, and η ensure physical monotonicity of degradation. Symmetric bounds on the interaction terms f and g allow both amplifying and compensating effects to be captured. Moderate upper bounds are used to prevent

Table 2
Bounds imposed on the empirical model parameters during the optimisation process.

Parameter	Lower bound	Upper bound
a	1×10^{-8}	1×10^{-1}
b	0.2	3.5
c	−0.5	2.0
d	0.0	5.0
γ	0.5	4.0
e	0.0	5.0
η	0.5	4.0
f	−1.0	2.0
g	−1.0	2.0

instability of the exponential term and reduce the risk of overfitting.

The optimisation procedure led to the identification of the parameters listed in Table 3.

The parameters obtained show the dominant role of cumulative energy x in the degradation process: $b > 1$ confirms a super-linear behaviour, consistent with the acceleration of degradation in the advanced stages of life. The contribution linked to dynamic stresses, described by C_{RMS} and the parameters d and γ, is significant and reflects the battery's sensitivity to intense power regimes and rapid transients. On the contrary, the term associated with the SoC variability has a very low weight, indicating that, under the operating conditions observed, SoC oscillations contribute less than cumulative energy throughput and current intensity. Finally, the presence of coupling terms allows the model to capture the interaction effects between energy throughput, load intensity, and SoC variability, improving the flexibility of the model while preserving physical interpretability.

3.2. Model accuracy on real data

Table 4 lists the performance of the proposed model in the three datasets (e.g., training, validation, test), expressed by RMSE and coefficient of determination R^2.

The model's performance is stable and consistent across all phases: the RMSE remains around 1.5×10^{-3} and the coefficient of determination R^2 remains close to 0.965. This indicates high predictive power and excellent generalisation with respect to data not used in the calibration phase. For completeness, the performance of the RF teacher model was also explicitly quantified. On the test dataset, the RF model obtained an RMSE of 2.8×10^{-4} and an R^2 equal to 0.9989, compared with an RMSE of 1.5×10^{-3} and an R^2 equal to 0.9655 for the proposed hybrid empirical model. As expected, the RF teacher achieves higher purely statistical accuracy; however, it does not provide a closed-form, continuous, monotonic, and physically interpretable degradation law. The proposed distilled empirical model, therefore, sacrifices a limited amount of predictive accuracy in exchange for optimisation-readiness, physical consistency, and direct applicability to long-term residential-scale system-level analyses.

Fig. 9 shows the comparison between the measured SoH and the SoH estimated by the proposed model. The two curves are almost

Table 3
Numerical values of the parameters identified for the empirical model.

Parameter	Value	Description
a	3.69×10^{-2}	Non-linear component of cumulative energy
b	1.95	Exponent of cumulative energy
c	-1.40×10^{-2}	Linear correction on x
d	1.53×10^{-3}	Weight of the term C_{RMS}
γ	1.69	Exponent of the term C_{RMS}
e	2.38×10^{-20}	Weight of the term σ_{SoC}
η	3.41	Exponent of the term σ_{SoC}
f	1.78×10^{-3}	Coupling term $x\,C_{\text{RMS}}$
g	-1.50×10^{-3}	Coupling term $x\sigma_{\text{SoC}}$

Table 4
Performance of the empirical model on experimental datasets.

Dataset	RMSE (−)	R^2 (−)
Training	0.001585	0.9649
Validation	0.001522	0.9651
Test	0.001530	0.9655

superimposed over the entire observation period. The model accurately reproduces the actual behaviour, without introducing non-physical oscillations, and maintains a monotonic trend consistent with degradation phenomena. It is worth noting that the RF model, which is used as the teacher in the distillation process, achieves even higher accuracy. However, it produces discontinuous trajectories that are not suitable for engineering applications. The distilled empirical model, therefore, represents an effective compromise between predictive accuracy and physical interpretability, and the comparable performance across three physically distinct batteries confirms that the proposed formulation captures general degradation trends, rather than battery-specific artifacts.

3.3. Comparison with other degradation models from the scientific literature

For further assessment of the proposed formulation, the identical residential operating dataset was employed to evaluate five degradation models reported in the literature. These models are based on cumulative energy or energy-related metrics and were originally calibrated on real, residential operating profiles such as the models proposed by Micea et al. [21], Liu et al. [22], Maheshwari et al. [23], Seger et al. [24], and Tang et al. [27].

Specifically, they were evaluated on the used dataset by applying their empirical equations, enabling a direct comparison with the proposed model. In contrast to the lab-based settings of the original studies, this work investigates a real-world PV-BESS system, incorporating practical operational complexities. Fig. 11 compares the monthly evolution of the SoH obtained with these models and with the proposed formulation against the measured reference curve.

From a quantitative perspective, the performance indices reported in Table 5 show a clear advantage of the proposed model over those available in the scientific literature. This improvement can be attributed to the ability of the proposed formulation to jointly account for cumulative energy throughput, dynamic stress, and SoC variability within a single analytical framework. In contrast, degradation models from the scientific literature often rely on a limited set of stress indicators or implicitly assume linear degradation trends. As a result, they struggle to capture the combined and non-linear effects of operating conditions, which become dominant during the middle and final stages of battery life. Furthermore, the distillation process based on the RF teacher constrains parameter identification to physically meaningful regions of the solution space. This improves generalisation capabilities and reduces systematic bias when the model is applied to real operating profiles.

It is worth noting that these models were applied to the used dataset using their empirical equations, allowing for a direct comparison with the proposed model. Unlike the lab-based environments of the referenced studies, our analysis focuses on a real-world PV-BESS setup, which introduces additional complexities and operational variability.

In addition to global metrics, the absolute mean annual error SoH provides a complementary and intuitive measure of model accuracy. This indicator, shown in Table 5, was evaluated monthly and is shown in Fig. 10.

Furthermore, Fig. 11 graphs the real SoH trend, comparing it with the SoH trend estimated using the proposed model and models from the scientific literature.

Seger et al. [24] and Liu et al. [22] models tend to underestimate the degradation in the intermediate phase and overestimate it in the final

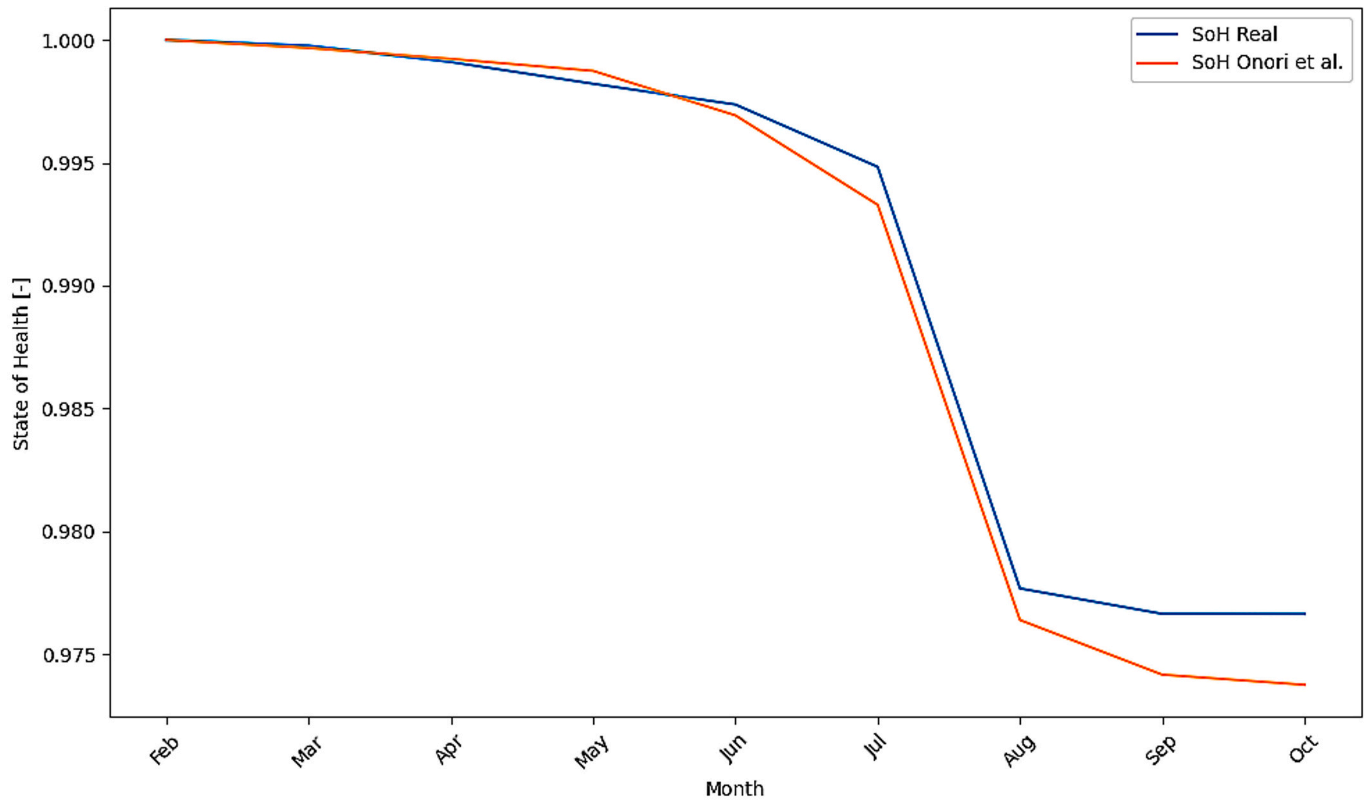

Fig. 9. SoH real vs SoH predicted.

Table 5
Quantitative comparison between the proposed degradation model and scientific literature models.

Model	R^2	RMSE (−)	Mean annual SoH error (%)
Proposed model	0.9655	0.00153	0.12
Micea et al. [21]	0.9266	0.00259	0.13
Maheshwari et al. [23]	0.8426	0.00327	0.30
Tang et al. [27]	0.7533	0.00409	0.16
Seger et al. [24]	0.6643	0.00527	0.45
Liu et al. [22]	0.6384	0.00495	0.42

phase, resulting in a SoH trajectory that is too linear and unable to reproduce the curvature of the real curve. Maheshwari et al.'s [23] model improves the representation of the first part of life, thanks to the explicit dependence on SoC and current, but still fails to fully capture the accelerated degradation observed in the last months, where the empirical model shows the greatest advantage. Micea et al. [21] tends to follow a similar trend to Maheshwari et al. [23], with more accurate representation during the earlier phases of degradation but showing more deviation during the final months. On the other hand, the Tang et al. [27] model exhibits a more pronounced error in the intermediate phase, where it significantly overestimates the degradation rate. The superior performance of the proposed model can be attributed to two key aspects. Firstly, the use of normalised cumulative energy x, dynamic stress C_{RMS}, and SoC variability σ_{SoC} in a unified analytical structure allows the combined effect of cycle depth, current intensity, and operating profile to be captured, without separating calendar and cyclic contributions. Secondly, the distillation mechanism from the RF teacher guides the parameter identification towards regions of the solution space that are well supported by the data, improving the representation of nonlinearities while preserving physical interpretability.

Overall, the results demonstrate that the proposed energy-based hybrid model is capable of accurately reproducing the degradation trends observed during the actual operation of BESS, where an accurate representation of the degradation curve is crucial. The high accuracy and physical interpretability make the proposed approach a strong candidate for integration into techno-economic analyses, optimal dispatch strategies, and estimates of the service life of storage systems in real-world, residential-based applications.

From an implementation perspective, the computational cost of the compared empirical models is similar, with running times on the order of seconds, meaning that computational time is not a distinguishing factor between the approaches. The model is not designed as an online diagnostic or real-time control tool, but as a system-level degradation model for techno-economic optimization and planning studies. The authors have clarified that the 24-h rolling window used for dynamic stress indicators aligns with the typical operational cycle of residential PV-BESS systems. Sensitivity analyses have shown that the model remains stable when the rolling-window length is adjusted, although this parameter should be recalibrated for systems with significantly different operating profiles, such as grid services or fast-cycling industrial storage.

4. Conclusions

This study presents and validates an empirical energy-based degradation model for Lithium-ion batteries, calibrated with real residential operating data from three independent 5 kWh BESS units. The model describes SoH evolution as an exponential function of three measurable operational indicators: normalised cumulative energy throughput, C_{RMS}, and σ_{SOC}. By integrating these variables into a unified formulation, the model captures the combined effects of energy usage, current stress, and operational variability without relying on the conventional separation between calendar and cycle aging.

A key contribution is the combination of a distillation-based calibration procedure with an interpretable empirical structure. First, a data-driven RF model is trained on the available data and then used to guide the identification of a closed-form degradation law. This

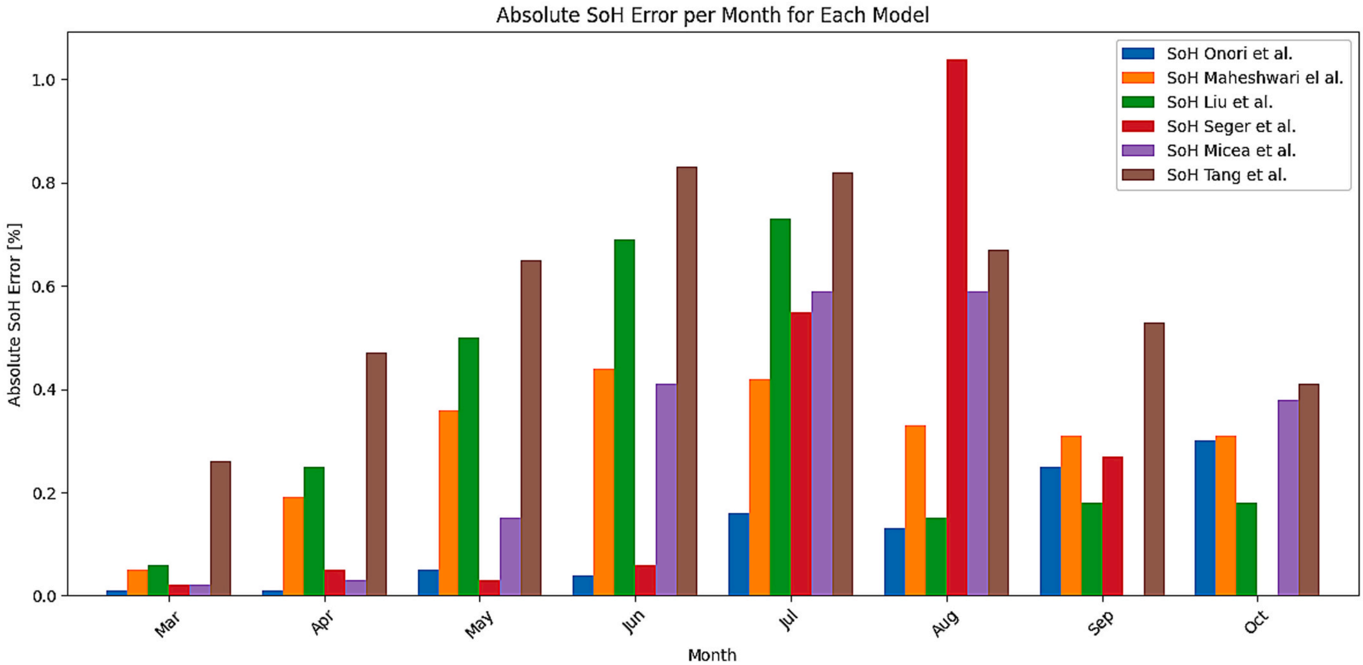

Fig. 10. Comparison of monthly absolute percentage errors of different SoH degradation models with respect to measured data.

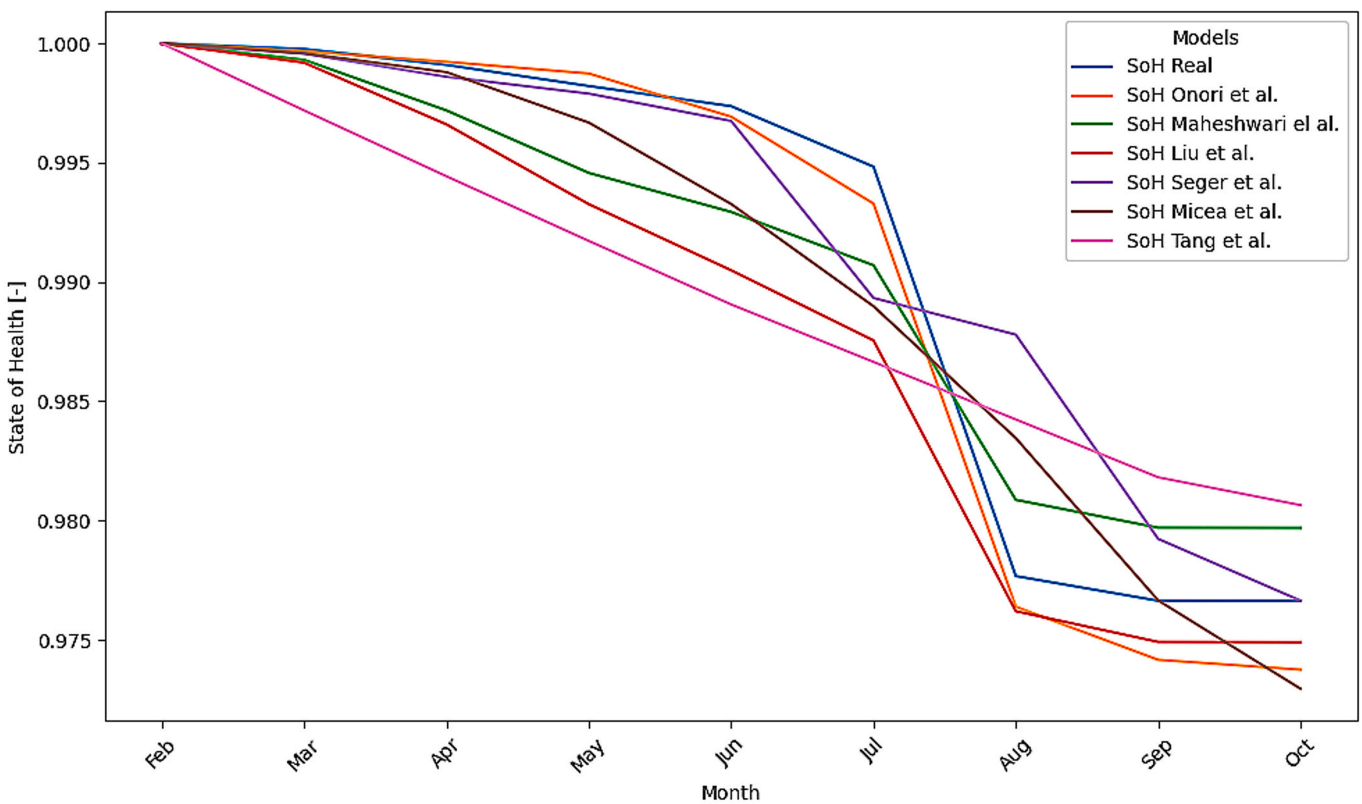

Fig. 11. Comparison between the real SoH trend and estimates obtained by applying five models found in the scientific literature (Seger et al. [24], Maheshwari et al. [23], Liu et al.[22], Micea et al. [21], Tang et al.[27]) and the proposed model.

procedure enables the resulting model to retain part of the predictive capability of the RF teacher while ensuring monotonicity, numerical stability, physical plausibility, and low computational cost. Validation on unseen systems confirms its good generalisation capability.

The proposed formulation achieves consistent performance across training, validation, and testing phases, with an RMSE on the order of 1.5×10^{-3} and $R^2 = 0.965$, while producing smooth and physically consistent SoH trajectories. Compared with existing energy-based models, including those by [21–24,27], it reduces the RMSE by more than 50% and provides a significantly improved representation of nonlinear degradation, particularly in the end-of-life region.

The model is intended as a system-level tool for direct integration into optimisation and techno-economic frameworks. In this respect, it helps bridge the gap between highly accurate data-driven approaches, including recent interpretable machine-learning models, and optimisation-oriented empirical formulations. Although interpretable data-driven models may achieve excellent predictive accuracy, they do not necessarily provide a closed-form, continuous, monotonic, and directly embeddable degradation law. The proposed approach, therefore, prioritises optimisation-readiness and physical consistency, while preserving part of the predictive strength of the RF teacher through distillation. Since the available dataset includes a limited number of physically independent systems, the proposed model should be interpreted as specifically applicable to integrated PV-BESSs operating under real-world conditions. Although the identified parameter values are application-specific, the model structure is transferable and can be recalibrated for different battery technologies and operating contexts.

It is worth noting that temperature, which is a well-known driver of battery degradation, was intentionally excluded to maintain the model's applicability in real-world scenarios with limited sensor availability. While this choice enhances practical usability, it may reduce accuracy under conditions where temperature has a significant impact on aging. Furthermore, the model is specifically tailored for residential PV-BESS systems; its application to other contexts, such as EVs or large grid-connected storage systems with markedly different charge–discharge profiles, falls outside the scope of this work. Future research will aim to extend the formulation to incorporate temperature effects, refine the model for integrated PV-BESS systems, and explore its adaptation to other variable load applications, including EVs.

Overall, the proposed approach offers a concise, robust, and scalable framework for degradation-aware operation and planning of BESSs.

CRediT authorship contribution statement

Filippo Onori: Writing – review & editing, Writing – original draft, Visualization, Software, Methodology, Investigation, Formal analysis, Data curation, Conceptualization. **Mosè Rossi:** Writing – review & editing, Writing – original draft, Visualization, Supervision, Methodology, Formal analysis, Conceptualization. **Gabriele Comodi:** Writing – review & editing, Writing – original draft, Supervision.

Declaration of competing interest

The authors declare that they have no known competing financial interests or personal relationships that could have appeared to influence the work reported in this paper.

Acknowledgements

The authors would like to thank BM Impianti S.r.l. for providing the real-world data of the PV-BESS systems, as well as the energy consumption profiles of their clients.

Data availability

The data that has been used is confidential.

References

[1] I. Charalampidis, Z. Vrontisi, D. Fragkiadakis, L. Nacke, J. Jew-ell, A regional model-based assessment of the socioeconomic impacts of EU climate neutrality pathways and the effectiveness of the just transition fund, Energy Policy 208 (2026) 114892, https://doi.org/10.1016/j.enpol.2025.114892. https://www.sciencedirect.com/science/article/pii/S0301421525003994.

[2] S. Koohi-Fayegh, M. Rosen, A review of energy storage types, applications and recent developments, J. Energy Storage 27 (2020) 101047, https://doi.org/10.1016/j.est.2019.101047. https://www.sciencedirect.com/science/article/pii/S2352152X19306012.

[3] M.I. Alemany, A. Castillejo-Cuberos, M. Negrete-Pincetic Álvaro Lorca, Assessing the feasibility of battery energy storage coupled to photovoltaic plants, participating on energy and ancillary services markets, through power system optimization and sub-hourly simulations, J. Energy Storage 140 (2025) 118993, https://doi.org/10.1016/j.est.2025.118993. https://www.sciencedirect.com/science/article/pii/S2352152X25037065.

[4] S. Massat, T. Franzelin, D. Dibbern, S. Rinderknecht, Development and analysis of a battery degradation model for use in mixed-integer linear programming, J. Energy Storage 150 (2026) 120511, https://doi.org/10.1016/j.est.2026.120511. https://www.sciencedirect.com/science/article/pii/S2352152X26001751.

[5] N. Collath, B. Tepe, S. Englberger, A. Jossen, H. Hesse, Aging aware operation of lithium-ion battery energy storage systems: a review, J. Energy Storage 55 (2022) 105634, https://doi.org/10.1016/j.est.2022.105634. https://www.sciencedirect.com/science/article/pii/S2352152X2201622X.

[6] A. Pena-Bello, M. Burer, M.K. Patel, D. Parra, Optimizing PV and grid charging in combined applications to improve the profitability of residential batteries, J. Energy Storage 13 (2017) 58–72, https://doi.org/10.1016/j.est.2017.06.002. https://www.sciencedirect.com/science/article/pii/S2352152X17301767.

[7] J. Figgener, P. Stenzel, K.-P. Kairies, J. Linßen, D. Haberschusz, O. Wessels, G. Angenendt, M. Robinius, D. Stolten, D.U. Sauer, The development of stationary battery storage systems in germany – a market review, J. Energy Storage 29 (2020) 101153, https://doi.org/10.1016/j.est.2019.101153. https://www.sciencedirect.com/science/article/pii/S2352152X19309442.

[8] D. Kucevic, B. Tepe, S. Englberger, A. Parlikar, M. Mühlbauer, O. Bohlen, A. Jossen, H. Hesse, Standard battery energy storage system profiles: analysis of various applications for stationary energy storage systems using a holistic simulation framework, J. Energy Storage 28 (2020) 101077, https://doi.org/10.1016/j.est.2019.101077. https://www.sciencedirect.com/science/article/pii/S2352152X19309016.

[9] M. Montaru, S. Fiette, J.-L. Koné, Y. Bultel, Calendar ageing model of Li-ion battery combining physics-based and empirical approaches, J. Energy Storage 51 (2022) 104544, https://doi.org/10.1016/j.est.2022.104544. https://www.sciencedirect.com/science/article/pii/S2352152X22005618.

[10] R.D. Deshpande, K. Uddin, Physics inspired model for estimating 'cycles to failure' as a function of depth of discharge for lithium ion batteries, J. Energy Storage 33 (2021) 101932, https://doi.org/10.1016/j.est.2020.101932. https://www.sciencedirect.com/science/article/pii/S2352152X20317680.

[11] J. Vetter, P. Novák, M. Wagner, C. Veit, K.-C. Möller, J. Besenhard, M. Winter, M. Wohlfahrt-Mehrens, C. Vogler, A. Hammouche, Aging mechanisms in lithium-ion batteries, J. Power Sources 147 (1) (2005) 269–281, https://doi.org/10.1016/j.jpowsour.2005.01.006. https://www.sciencedirect.com/science/article/pii/S0378775305000832.

[12] T. Rahman, T. Alharbi, Exploring lithium-ion battery degradation: a concise review of critical factors, impacts, data-driven degradation estimation techniques, and sustainable directions for energy storage systems, Batteries 10 (7) (2024), https://doi.org/10.3390/batteries10070220. https://www.mdpi.com/2313-0105/10/7/220.

[13] G. Sordi, D. Luder, W. Li, D.U. Sauer, A. Casalegno, C. Rabissi, Investigation of calendar aging of lithium-ion battery through physical models with ex-situ validation, J. Power Sources 615 (2024) 235076, https://doi.org/10.1016/j.jpowsour.2024.235076. https://www.sciencedirect.com/science/article/pii/S0378775324010280.

[14] P. Keil, S.F. Schuster, J. Wilhelm, J. Travi, A. Hauser, R.C. Karl, A. Jossen, Calendar aging of lithium-ion batteries, J. Electrochem. Soc. 163 (9) (2016) A1872, https://doi.org/10.1149/2.0411609jes.

[15] T. Waldmann, M. Wilka, M. Kasper, M. Fleischhammer, M. Wohlfahrt-Mehrens, Temperature dependent aging mechanisms in lithium-ion batteries – a post-mortem study, J. Power Sources 262 (2014) 129–135, https://doi.org/10.1016/j.jpowsour.2014.03.112. https://www.sciencedirect.com/science/article/pii/S0378775314004352.

[16] S.F. Schuster, T. Bach, E. Fleder, J. Müller, M. Brand, G. Sextl, A. Jossen, Nonlinear aging characteristics of lithium-ion cells under different operational conditions, J. Energy Storage 1 (2015) 44–53, https://doi.org/10.1016/j.est.2015.05.003. https://www.sciencedirect.com/science/article/pii/S2352152X15000092.

[17] S. Barcellona, L. Piegari, Effect of current on cycle aging of lithium ion batteries, J. Energy Storage 29 (2020) 101310, https://doi.org/10.1016/j.est.2020.101310. https://www.sciencedirect.com/science/article/pii/S2352152X19314574.

[18] J. de Hoog, J.-M. Timmermans, D. Ioan-Stroe, M. Swier-czynski, J. Jaguemont, S. Goutam, N. Omar, J. Van Mierlo, P. Van Den Bossche, Combined cycling and calendar capacity fade modelling of a nickel-manganese-cobalt oxide cell with real-life profile validation, Appl. Energy 200 (2017) 47–61, https://doi.org/10.1016/j.apenergy.2017.05.018. https://www.sciencedirect.com/science/article/pii/S0306261917305251.

[19] M. Schimpe, M.E. von Kuepach, M. Naumann, H.C. Hesse, K. Smith, A. Jossen, Comprehensive modelling of temperature-dependent degra-dation mechanisms in lithium iron phosphate batteries, J. Electrochem. Soc. 165 (2) (2018) A181, https://doi.org/10.1149/2.1181714jes.

[20] P.M. Attia, A. Bills, F. Brosa Planella, P. Dechent, G. dos Reis, M. Dubarry, P. Gasper, R. Gilchrist, S. Greenbank, D. Howey, O. Liu, E. Khoo, Y. Preger, A. Soni, S. Sripad, A.G. Stefanopoulou, V. Sulzer, Review—"knees" in lithium-ion battery aging trajectories, J. Electrochem. Soc. 169 (6) (2022) 060517, https://doi.org/10.1149/1945-7111/ac6d13.

[21] M.V. Micea, L. Ungurean, G.N. Cârstoiu, V. Groza, Online state-of-health assessment for battery management systems, IEEE Trans. Instrum. Meas. 60 (6) (2011) 1997–2006, https://doi.org/10.1109/TIM.2011.2115630.

[22] M. Liu, W. Li, C. Wang, M.P. Polis, L.Y. Wang, J. Li, Reliability evaluation of large scale battery energy storage systems, IEEE T. Smart Grid 8 (6) (2017) 2733–2743, https://doi.org/10.1109/TSG.2016.2536688.

[23] A. Maheshwari, N.G. Paterakis, M. Santarelli, M. Gibescu, Optimizing the operation of energy storage using a non-linear lithium-ion battery degradation model, Appl. Energy 261 (2020) 114360, https://doi.org/10.1016/j.apenergy.2019.114360. https://www.sciencedirect.com/science/article/pii/S0306261919320471.

[24] P.V. Seger, R. Rigo-Mariani, P.-X. Thivel, D. Riu, A storage degradation model of Li-ion batteries to integrate aging effects in the optimal management and design of an isolated microgrid, Appl. Energy 333 (2023) 120584, https://doi.org/10.1016/j.apenergy.2022.120584. https://www.sciencedirect.com/science/article/pii/S0306261922018414.

[25] S. Son, S. Jeong, E. Kwak, J. Hyeong Kim, K.-Y. Oh, Integrated framework for SOH estimation of lithium-ion batteries using multiphysics features, Energy 238 (2022) 121712, https://doi.org/10.1016/j.energy.2021.121712. https://www.sciencedirect.com/science/article/pii/S0360544221019605.

[26] M. Bao, D. Liu, Y. Wu, Z. Wang, J. Yang, L. Lan, Q. Ru, Interpretable machine learning prediction for Li-ion battery's state of health based on electrochemical impedance spectroscopy and temporal features, Electrochim. Acta 494 (2024) 144449, https://doi.org/10.1016/j.electacta.2024.144449. https://www.sciencedirect.com/science/article/pii/S001346862400690X.

[27] X. Tang, C. Zou, K. Yao, J. Lu, Y. Xia, F. Gao, Aging trajectory prediction for lithium-ion batteries via model migration and Bayesian Monte Carlo method, Appl. Energy 254 (2019) 113591, https://doi.org/10.1016/j.apenergy.2019.113591. https://www.sciencedirect.com/science/article/pii/S0306261919312656.

[28] H. Lyu, Y. Li, C.J. Jafta, C.A. Bridges, H.M. Meyer, A. Bori-sevich, M. P. Paranthaman, S. Dai, X.-G. Sun, Bis(trimethylsilyl) 2-fluoromalonate derivatives as electrolyte additives for high voltage lithium ion batteries, J. Power Sources 412 (2019) 527–535, https://doi.org/10.1016/j.jpowsour.2018.11.083. https://www.sciencedirect.com/science/article/pii/S0378775318313387.

[29] M.G. Hennessy, I.R. Moyles, Asymptotic reduction and homogenization of a thermo-electrochemical model for a lithium-ion battery, Appl. Math. Model. 80 (2020) 724–754, https://doi.org/10.1016/j.apm.2019.11.018. https://www.sciencedirect.com/science/article/pii/S0307904X19306912.

[30] ARERA, Autorità di regolazione per energia reti e ambiente. https://www.arera.it/ accessed: 2026-06-11.